Solutions for vectorial beam coupling under ac field in cubic photorefractive crystals

B. I. Sturman
Institute of Automation and Electrometry, Koptyg Ave 1, 630090 Novosibirsk, Russia

O. S. Filippov
Department of Physics, University of Osnabrück, D-49069 Osnabrück, Germany

(Received 1 May 2003; published 26 September 2003)

We develop a theory of vectorial wave coupling in cubic photorefractive crystals placed in an alternating ac field to enhance the nonlinear response. It is proven in the general case that despite essential differences between the diffusion and the ac nonlocal responses, the latter keeps the light interference fringes straight during the interaction. This fundamental feature allows, under certain restrictions, to reduce the nonlinear problem of vectorial coupling to the known linear problem of vectorial Bragg diffraction from a spatially uniform grating, which admits an exact solution. As a result, the nonlinear vectorial problem can be effectively solved for a number of practically important cases. These cases include nontrivial polarization effects and also the high-contrast effects. The presence of conservation laws involving the polarization degrees of freedom is shown. A number of particular cases relevant to experiments with BTO crystals are considered.

DOI: 10.1103/PhysRevE.68.036613 PACS number(s): 42.70.Nq, 42.65.Hw

I. INTRODUCTION

Photorefractive (PR) wave coupling has been the subject of many studies [1,2]. Usually, the strongest wave interactions occur in PR ferroelectrics which are highly anisotropic. Unfortunately, the nonlinear PR response of ferroelectrics is not sufficiently fast for optical applications. Many efforts have been made to find faster photorefractive materials [1,2]. Nowadays, cubic crystals of the sillenite family (BSO, BTO, and BGO) and also cubic semiconductors (CdTe, GaAs, and InP) meet the speed requirements fully.

A common weak point of the above fast materials is their insufficiently high nonlinear response. Two techniques (dc and ac) have been proposed to enhance this response [3,4]. Both of these exploit applied electric fields. In the dc case the field is constant and the interacting light waves are slightly detuned in frequency. In the ac case, which is proven to be most useful for applications, an external electric field oscillates in time and no frequency detuning is necessary to introduce between the light waves. The efficiency of the ac technique depends on the temporal profile of the ac field [5]. The best enhancement occurs for a square-wave profile when the field changes its sign periodically.

Considerable progress in improving the photorefractive characteristics of the sillenites has been made during the last decade [6,7]. The fabrication of thin and long BSO and BTO crystals has allowed to increase the amplitude of the ac field up to 50 kV/cm, to decrease the response time in cw experiments to microseconds, and to demonstrate a variety of strong nonlinear effects relevant to applications such as fast phase conjugation [8], generation of surface light waves [9,10], time separated recording and readout processes [11], and the liner detection of weak signals [12].

The main problem, and the main characteristic feature, in describing the PR wave phenomena in cubic crystals is the vectorial character of the optical coupling. In other words, the energy and polarization changes cannot generally be separated from each other. The sensitivity of the optical phenomena to the polarization degrees of freedom, and also to the crystal cut, can definitely be regarded as a property useful for applications. The presence of strong nonlinear phenomena, a high spatial symmetry of the optically isotropic medium, and an apparent simplicity of formulation of the nonlinear problems is a challenge for theorists in the field of photorefraction.

Despite numerous publications, theoretical description of the PR phenomena in cubic crystals remained till recently very fragmental. A number of papers dealt with an analysis of vectorial Bragg diffraction from a uniform grating of the space-charge field [13–16]. Most of these papers used various approximations or numerical methods. The effects of weak two-wave coupling were considered in Refs. [17–19] using the thin-crystal approximation. The corresponding results are applicable to a very restricted amount of experimental data. Various aspects of the enhancement problem were considered in Refs. [3–5,20,21]. The nonlinear optical effects lay outside the main stream of these studies. Considerable efforts have been made to describe the contributions to the PR response caused by the elasto-optic effect, see, e.g., Refs. [22–25]. A number of publications aimed at the analysis of strong nonlinear effects caused by the enhanced PR response [9,26–28]. These papers restricted themselves to formulation of the initial equations for wave amplitudes (which include many model parameters and experimental characteristics) and some simulations of these equations. The corresponding numerical results give usually no insight into the nonlinear phenomena under study.

An important step in describing the vectorial coupling has been made recently in Refs. [29,30]. The authors have found an adequate theoretical scheme capable of combining the general analytical methods with incorporation of the factual data on the PR response. The analytical merits are based on the systematic use of the properties of spatial symmetry and the apparatus of Pauli matrices [31]. This approach has allowed to describe in a uniform manner a number of important vectorial effects: the above mentioned vectorial Bragg

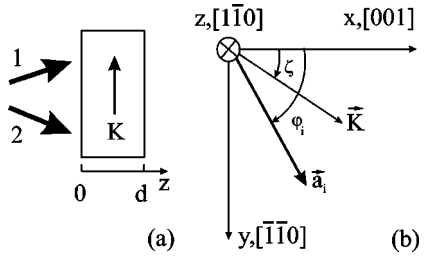

FIG. 1. (a) Schematic of a two-wave coupling experiment. (b) Orientation of the main 2D vectors about the crystal axes; $\vec{a}_i$ is the amplitude of the ith wave ($i=1,2$).

diffraction [15], the angular distribution of the light-induced scattering in BTO and BSO crystals [29,30], and the linear detection of weak signals by means of polarization filtering [32,33].

The purpose of this paper is to describe the progress made in investigation (analytical and numerical) of the characteristics of vectorial coupling in the ac case. Our findings can be considered as an extension of the classical results obtained for the case of scalar beam coupling [1,2] to the vectorial case. The text is structured as follows: First, we formulate the vectorial coupling equations and provide the reader with the necessary information on the nonlinear ac response. It is proven then in the general case that the light fringes remain straight inside the crystal in spite of coupling effects and the structural differences between the vectorial and scalar equations. Further we introduce certain simplifying assumptions for the coupling coefficients and specify the conditions of their validity. Next we show that the nonlinear coupling problem can be reduced to the known linear problem of the vectorial Bragg diffraction by a renormalization of the propagation coordinate. With this renormalization performed the vectorial problem admits an exact solution in the whole-contrast range. This procedure allows also to reveal the presence of conservation laws involving essentially the polarization degrees of freedom. Finally, we apply the exact solutions obtained to a number of important particular cases.

II. BASIC RELATIONS

A. Vectorial diffraction equation

Let two light waves 1 and 2 be coupled in a cubic PR crystal via diffraction from the light-induced grating of space-charge field whose grating vector $\vec{K}$ is the difference of the light wave vectors, see Fig. 1(a). As soon as the light absorption is neglected, the total intensity of the waves does not depend on the propagation coordinate z and we can normalize the vectorial complex wave amplitudes $\vec{a}_1,\vec{a}_2$ in such a way that $|\vec{a}_1|^2+|\vec{a}_2|^2=1$. We denote the amplitude of the light-induced space-charge field as E_K; it is generally a function of z. With this notation and within the conventional paraxial approximation, the set of equations describing vectorial Bragg diffraction from the grating can be presented in the following general and compact form [29]:

$$(\partial_z - i\boldsymbol{\kappa}\cdot\hat{\boldsymbol{\sigma}})\vec{a}_1 = iE_K(\nu_0+\boldsymbol{\nu}\cdot\hat{\boldsymbol{\sigma}})\vec{a}_2, \tag{1}$$

$$(\partial_z - i\boldsymbol{\kappa}\cdot\hat{\boldsymbol{\sigma}})\vec{a}_2 = iE_K^*(\nu_0+\boldsymbol{\nu}\cdot\hat{\boldsymbol{\sigma}})\vec{a}_1. \tag{2}$$

Here $\boldsymbol{\kappa}=(\kappa_1,-\rho,\kappa_3)$ (ρ is the rotatory power) and $\boldsymbol{\nu}=(\nu_1,0,\nu_3)$ are known real three-dimensional (3D) vectors, ν_0 is a known real scalar, $\hat{\boldsymbol{\sigma}}=(\sigma_1,\sigma_2,\sigma_2)$ the standard set of 2×2 Pauli matrices, see Ref. [31], and $\vec{a}_{1,2}$ are 2D vectors with x and y components (note: the 3D quantities with 1,2,3 components are denoted by bold letters). The vector $\boldsymbol{\kappa}$ characterizes the linear optical properties; its components $\kappa_{1,3}$ account for the changes of the optical permittivity induced by a uniform applied electric field via the linear electro-optic effect and the component $\kappa_2=-\rho$ accounts for the effect of optical activity (if it is present in the crystal). The vector $\boldsymbol{\nu}$ and the scalar ν_0 are responsible for the anisotropic and isotropic parts of diffraction, respectively. The fact that the component $\nu_2=0$ means that the light-induced space-charge field does not produce any changes of the rotatory power ρ. Set (1),(2) can be considered as an extension of the known scalar Kogelnik theory to the vectorial case. One can check that the Hermitian property of the σ matrices ensures the conservation of the total wave intensity, i.e.,

$$I_0=|\vec{a}_1|^2+|\vec{a}_2|^2=1. \tag{3}$$

This is the integral of Eqs. (1) and (2). In the case of a uniform grating, $E_K(z)=\text{const}$, set (1),(2) admits nontrivial exact general solutions for the vectorial diffraction [15,29].

Throughout this paper we are dealing with cubic crystals of the point groups 23 and $\bar{4}3m$; this is sufficient for all visible practical purposes. The first case is relevant to the sillenites (BSO, BTO, and BGO) whereas the second one corresponds to semiconductors GaAs, CdTe, InP, and others. The electro-optic properties of the above cubic crystals are the same in symmetry. At the same time, crystals of the point group 23 are optically active (the rotatory power $\rho\neq0$) in contrast to crystals belonging to the $\bar{4}3m$ group.

The coefficients $\kappa_{1,3}$ and $\nu_{0,1,3}$ entering Eqs. (1) and (2) can be calculated for any orientation of the applied field $\vec{E}_0$ and the grating vector $\vec{K}$ about the crystal axes. Below we restrict ourselves to the case when the propagation axis z is directed along $[1\bar{1}0]$, see Fig. 1(b), and the applied field $\vec{E}_0$ is parallel to the grating vector $\vec{K}$; this covers most of the topical situations. Then the components $\kappa_{1,3}$ can be presented in the form

$$\kappa_1=sE_0\sin\zeta, \qquad \kappa_3=-\frac{sE_0}{2}\cos\zeta, \tag{4}$$

where ζ is the angle between $\vec{K}$ and the [001] crystal axis, $s=-\pi n_0^3 r_{41}/\lambda$, n_0 the nonperturbed refractive index, r_{41} the only nonzero electro-optic constant, and λ the wavelength. The sign of E_0 can be positive and negative in Eqs. (4). The coefficients $\nu_{0,1,3}$ include generally not only electro-optic but also elasto-optic contributions, the latter can sometimes be of importance. If we neglect the elasto-optic contributions, then

$$\nu_0=\frac{s}{2}\cos\zeta, \quad \nu_1=s\sin\zeta, \quad \nu_3=-\frac{s}{2}\cos\zeta. \tag{5}$$

The data on $\nu_{0,1,3}(\zeta)$ with the elasto-optic contributions taken into account can be found in Ref. [29].

Three particular cases are especially important for the experiment:

(1) The transverse (T) geometry, $\vec{K},\vec{E}_0\perp[001]$, i.e., $\zeta=90°$. Here $\kappa_1=sE_0,\kappa_3=0$. The elasto-optic contributions renormalize here slightly the electro-optic constant r_{41}, therefore $\nu_0=0$, $\nu_1\simeq s$, and $\nu_3=0$.

(2) The longitudinal (L) optical configuration, $\vec{K},\vec{E}_0\|[001]$, i.e., $\zeta=0$. Here $\kappa_1=0,\kappa_3=sE_0/2$. The elasto-optic contributions are absent here, hence $\nu_0=s/2,\nu_1=0$, and $\nu_3=-s/2$.

(3) The diagonal (D) geometry, $\vec{K},\vec{E}_0\|[111]$, $\zeta=\arctan(\sqrt{2})\simeq 54.7°$. Here $\kappa_1=\sqrt{2}\,sE_0$, $\kappa_3=-sE_0/2\sqrt{3}$. The elasto-optic contributions to $\nu_{0,1,3}$ are clearly pronounced here, they can give up to 30% corrections to the values given by Eqs. (5).

There are a large number of optical configurations that are equivalent (for symmetry reasons) to the above considered, these configurations are listed in Ref. [29].

Commenting on the above relations for the optical configurations, we mention first that the isotropic part of diffraction is absent in the T geometry. This case is maximally different from the familiar scalar diffraction. Furthermore, there is no case when the anisotropic part of diffraction is absent or small as compared to the isotropic part. Hence, strong polarization effects are expected in cubic PR crystals.

It is important for what follows that the vectors $\boldsymbol{\kappa}$ and $\boldsymbol{\nu}$ are parallel to each other in the L and T geometries if the optical activity is absent (crystals of the $\bar{4}3m$ point group). In the sillenites (where $\rho\neq 0$) $\boldsymbol{\kappa}$ is approximately parallel to $\boldsymbol{\nu}$ when $s|E_0|\gg\rho$, which means suppression of optical activity by the applied field. This situation is typical of ac experiments with BTO crystals, where $\rho\simeq 6.5°\ \mathrm{mm}^{-1}\simeq 1.1\ \mathrm{cm}^{-1}$, $|s|\simeq 4\times 10^{-4}\ \mathrm{V}^{-1}$, and the amplitude $|E_0|$ ranges from 10 to 50 kV/cm. In the D geometry, it is necessary to be careful when using the approximation $\boldsymbol{\kappa}\|\boldsymbol{\nu}$ because of noticeable elasto-optic contributions to $\boldsymbol{\nu}_{1,3}$.

B. Nonlinear ac response

To complete set (1),(2), it is necessary to specify the PR nonlinear response, i.e., to express the grating amplitude E_K through the light amplitudes $\vec{a}_{1,2}$. We assume that the grating formation occurs under the action of a quickly oscillating square-wave shaped applied electric field of the amplitude $|E_0|$ which is much larger than the characteristic diffusion field E_D. This ac method for enhancement of the PR response is the most useful for applications. The necessary relation for the grating amplitude can be represented in the form [1,34,37,38]

$$E_K=-iQf|E_0|(\vec{a}_1\cdot\vec{a}_2^{\,*}). \tag{6}$$

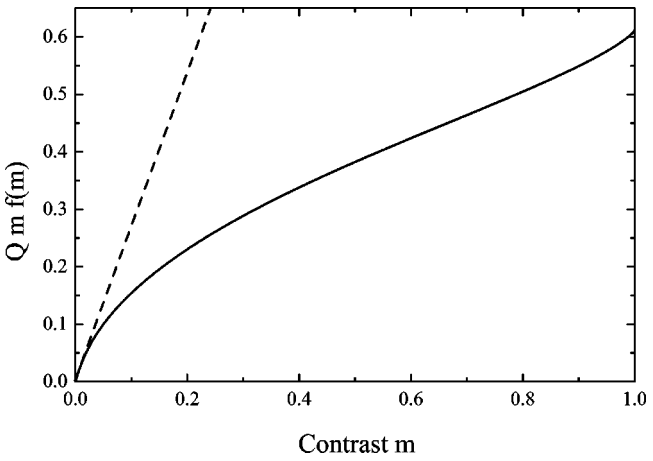

FIG. 2. The function $Qmf(Q,m)$ for $Q=6$; the dashed line shows the linear approximation.

Here $Q=Q(K,|E_0|)$ is a dimensionless factor considerably larger than the one that has the meaning of the quality factor for a space-charge wave with the wave vector $\vec{K}$ [34] and $f=f(m)$ is a function of the contrast of the light interference pattern $m=2|\vec{a}_1\cdot\vec{a}_2^{\,*}|$.

Figure 2 shows a representative contrast dependence of the product $Qmf(m)$, see Ref. [39] for more details. In the low-contrast limit, $m\lesssim m_c\approx 0.05\ll 1$, we have $f\simeq 1$; this limit corresponds to the known result for the ac enhancement of the PR response [1,4]. Within the interval $m_c\lesssim m<1$ the function $f(m)$ is decreasing which means decreasing efficiency of the ac enhancement. The critical value of the contrast, m_c, can roughly be estimated as $\approx Q^{-2}$. The product $mf(m)$ experiences saturation on the level of $\approx Q^{-1}$ when $m\to 1$, i.e., the value of the grating amplitude E_K is saturated on the level of $|E_0|$. Actually, the saturation of $E_K(m)$ for $m>m_c$ is payment for the steep linear growth of $E_K(m)$ in the region of small contrast. The saturation of $E_K(m)$ is accompanied by an efficient excitation of the higher spatial harmonics, $E_{2K},E_{3K},\ldots$. In ac experiments with the sillenite crystals the quality factor Q ranges typically from 4 to 6; the function $Qmf(Q,m)$ does not experience strong changes here. We shall use, in what follows, the representative dependence of Fig. 2 for modeling of vectorial coupling.

The presence of the imaginary unit i in Eq. (6) means that the fundamental grating of the space-charge field, $E_K\exp(i\vec{K}\cdot\vec{r})+\mathrm{c.c.}$, is shifted by a quarter of a period with respect to the light intensity grating, i.e., the PR response is nonlocal (gradientlike). This property is well known for the ac enhancement in the low-contrast limit; it has important consequences for wave coupling in the whole-contrast region, $0<m<1$.

III. ANALYSIS AND SIMPLIFICATION OF VECTORIAL EQUATIONS

First, using Eq. (6) for E_K, we obtain from Eqs. (1) and (2) the closed set of equations for $\vec{a}_{1,2}$,

$$(\partial_z-i\boldsymbol{\kappa}\cdot\hat{\boldsymbol{\sigma}})\,\vec{a}_1=Q|E_0|f(m)(\vec{a}_1\cdot\vec{a}_2^{\,*})(\nu_0+\boldsymbol{\nu}\cdot\hat{\boldsymbol{\sigma}})\vec{a}_2, \tag{7}$$

$$(\partial_z - i\boldsymbol{\kappa}\cdot\hat{\boldsymbol{\sigma}})\vec{a}_2 = -Q|E_0|f(m)(\vec{a}_1^*\cdot\vec{a}_2)(\nu_0+\boldsymbol{\nu}\cdot\hat{\boldsymbol{\sigma}})\vec{a}_1, \tag{8}$$

where, as earlier, $m=2|\vec{a}_1\cdot\vec{a}_2^*|$.

In the next step we prove that the light interference fringes experience neither bending nor tilting inside the crystal despite the coupling effects. This is an important generalization of the property of beam coupling known for the nonlocal response in the scalar case on the vectorial case. We note first that the light intensity pattern inside the crystal is proportional to $[1+m\cos(\vec{K}\cdot\vec{r}+\Phi)]$, where $\Phi=\arg(\vec{a}_1\cdot\vec{a}_2^*)$ and $\vec{K}\perp\mathbf{z}$. If $\Phi(z)=\text{const}$, the light fringes remain perpendicular to the input face. Multiplying the vectorial equations (7) and (8) scalarly by $\vec{a}_2^*$ and $\vec{a}_1^*$, respectively, combining the obtained scalar relations, and using the Hermitian property of the σ matrices, we obtain the necessary equality $\partial_z\Phi_z=0$. This general property of the light fringes was missed in Ref. [29]. Being very simple, it simplifies greatly the following considerations.

Since the phase $\Phi(z)=\text{const}$, we can put it equal to zero without any loss of generality. In other words, one can make the replacement $\vec{a}_{1,2}\to\vec{a}_{1,2}\exp(\pm i\Phi/2)$ to work then with new fully equivalent vectorial light amplitudes. Therefore, from now on we set $\vec{a}_1\cdot\vec{a}_2^*=m/2$.

At this point, we need to make the main approximation of this paper, namely, $\boldsymbol{\kappa}\|\boldsymbol{\nu}$. The situations where it is justified have been considered in the preceding section. Within this approximation, the set of nonlinear equations (7),(8) admits exact solutions while the polarization properties of beam coupling remain far from trivial.

To get rid of the linear terms in Eqs. (7) and (8), we perform the unitary transformation from $\vec{a}_{1,2}$ to the amplitudes $\vec{b}_{1,2}$,

$$\vec{a}_{1,2}=\exp[i(\boldsymbol{\kappa}\cdot\hat{\boldsymbol{\sigma}})z]\vec{b}_{1,2}. \tag{9}$$

This transformation does not change the scalar products; in particular, $|\vec{a}_{1,2}(z)|^2=|\vec{b}_{1,2}(z)|^2$ and $\vec{a}_1(z)\cdot\vec{a}_2^*(z)=\vec{b}_1(z)\cdot\vec{b}_2^*(z)\equiv m(z)/2$. It does not change also the input values of the amplitudes, $\vec{b}_{1,2}(0)=\vec{a}_{1,2}(0)$. After the unitary transformation we have (using the property $\boldsymbol{\kappa}\|\boldsymbol{\nu}$)

$$\partial_z\vec{b}_1=+(Q|E_0|/2)mf(m)(\nu_0+\boldsymbol{\nu}\cdot\hat{\boldsymbol{\sigma}})\vec{b}_2, \tag{10}$$

$$\partial_z\vec{b}_2=-(Q|E_0|/2)mf(m)(\nu_0+\boldsymbol{\nu}\cdot\hat{\boldsymbol{\sigma}})\vec{b}_1. \tag{11}$$

Finally, we transfer from the propagation coordinate z to the variable ξ (an effective coordinate),

$$\xi=(Q|E_0|/2)\int_0^z m(z')f[m(z')]dz', \tag{12}$$

to obtain instead of Eqs. (10) and (11)

$$\partial_\xi\vec{b}_1=+(\nu_0+\boldsymbol{\nu}\cdot\hat{\boldsymbol{\sigma}})\vec{b}_2, \tag{13}$$

$$\partial_\xi\vec{b}_2=-(\nu_0+\boldsymbol{\nu}\cdot\hat{\boldsymbol{\sigma}})\vec{b}_1. \tag{14}$$

This set of differential equations is already *linear*, it describes vectorial diffraction from a uniform grating and admits an exact general solution in the terms of the effective coordinate ξ. The nonlinear part of the problem is therefore reduced to determination of the function $\xi(z)$, which is monotonically increasing starting from zero, $\xi(0)=0$. As soon as the dependence $m(\xi)$ is found from Eqs. (10) and (11), the function $\xi(z)$ can be obtained by an integration (analytical or numerical).

IV. EXACT SOLUTIONS

It is not difficult to check, see also Refs. [15,29], that the exact solution of Eqs. (13) and (14) with the boundary conditions $\vec{b}_{1,2}(0)=\vec{b}_{1,2}^0$ is

$$\vec{b}_1=[\cos(\nu_0\xi)\cos(\nu\xi)-(\mathbf{n}\cdot\hat{\boldsymbol{\sigma}})\sin(\nu_0\xi)\sin(\nu\xi)]\vec{b}_1^0 + [\sin(\nu_0\xi)\cos(\nu\xi)+(\mathbf{n}\cdot\hat{\boldsymbol{\sigma}})\cos(\nu_0\xi)\sin(\nu\xi)]\vec{b}_2^0, \tag{15}$$

$$\vec{b}_2=-[\sin(\nu_0\xi)\cos(\nu\xi)+(\mathbf{n}\cdot\hat{\boldsymbol{\sigma}})\cos(\nu_0\xi)\sin(\nu\xi)]\vec{b}_1^0 + [\cos(\nu_0\xi)\cos(\nu\xi)-(\mathbf{n}\cdot\hat{\boldsymbol{\sigma}})\sin(\nu_0\xi)\sin(\nu\xi)]\vec{b}_2^0, \tag{16}$$

where $\nu=|\boldsymbol{\nu}|$ is the scalar characterizing the strength of anisotropic diffraction and $\mathbf{n}=\boldsymbol{\nu}/\nu$ is the real unit 3D vector. Two spatial frequencies ν_0 and ν are present in Eqs. (15) and (16). One can check furthermore that $|\vec{b}_1(\xi)|^2+|\vec{b}_1(\xi)|^2=1$.

Using Eqs. (15) and (16), we find the contrast $m=2(\vec{b}_1\cdot\vec{b}_2^*)$ as a function of ξ,

$$m=m_0\cos(2\nu_0\xi)\cos(2\nu\xi)-W_0\sin(2\nu_0\xi)\cos(2\nu\xi) - F_0\cos(2\nu_0\xi)\sin(2\nu\xi)-P_0\sin(2\nu_0\xi)\sin(2\nu\xi), \tag{17}$$

where $m_0=m(0)$ is the input value of the contrast and W_0, F_0,P_0 are the input values of the following real scalar characteristics of the vectorial coupling:

$$W=|\vec{b}_1|^2-|\vec{b}_2|^2,\quad F=\langle 1|(\mathbf{n}\cdot\hat{\boldsymbol{\sigma}})|1\rangle-\langle 2|(\mathbf{n}\cdot\hat{\boldsymbol{\sigma}})|2\rangle,$$
$$P=2\,\mathrm{Re}\,\langle 1|(\mathbf{n}\cdot\hat{\boldsymbol{\sigma}})|2\rangle. \tag{18}$$

We have used here the conventional quantum-mechanic notation for the matrix elements, e.g., $\langle 1|(\mathbf{n}\cdot\hat{\boldsymbol{\sigma}})|2\rangle=\vec{b}_1^*\cdot(\mathbf{n}\cdot\hat{\boldsymbol{\sigma}})\vec{b}_2$. As follows from Eqs. (18), W is the normalized difference of the beam intensities, F characterizes the polarization freedom degrees, and P describes a correlation of polarizations in beams 1 and 2. To make this assertion more clear, we recall, see also Refs. [35,36], that the real 3D vector $\mathbf{S}_i=\langle i|\hat{\boldsymbol{\sigma}}|i\rangle/|\vec{b}_i|^2$ $(i=1,2)$ is the unit Stokes vector for ith beam, its components $(S_i)_{1,3}$ characterize the degree of linear polarization and the component $(S_i)_2$ characterizes the

degree of ellipticity. In what follows, we shall provide the reader with particular examples of polarization characterization.

The structure of Eq. (17) makes us to expect that explicit relations for m, W, F, and P, which follow from Eqs. (15) and (16), form a closed set. It is not difficult to find out that

$$W = m_0 \sin(2\nu_0\xi)\cos(2\nu\xi) + W_0 \cos(2\nu_0\xi)\cos(2\nu\xi) - F_0 \sin(2\nu_0\xi)\sin(2\nu\xi) + P_0 \cos(2\nu_0\xi)\sin(2\nu\xi), \tag{19}$$

$$F = m_0 \cos(2\nu_0\xi)\sin(2\nu\xi) - W_0 \sin(2\nu_0\xi)\sin(2\nu\xi) + F_0 \cos(2\nu_0\xi)\cos(2\nu\xi) + P_0 \sin(2\nu_0\xi)\cos(2\nu\xi), \tag{20}$$

$$P = -m_0 \sin(2\nu_0\xi)\sin(2\nu\xi) - W_0 \cos(2\nu_0\xi)\sin(2\nu\xi) - F_0 \sin(2\nu_0\xi)\cos(2\nu\xi) + P_0 \cos(2\nu_0\xi)\cos(2\nu\xi). \tag{21}$$

From here one finds algebraically that the quantity

$$I_p = m^2 + W^2 + F^2 + P^2 \tag{22}$$

remains constant across the crystal, i.e., I_p is a new (in addition to I_0) integral of set (1),(2). It involves the polarization degrees of freedom. One can show that, depending on polarizations of the input beams, I_p ranges from 1 to 2. It is worth mentioning that the unitary transformation (9) does not change the quantities W, F, and P, defined by Eqs. (18); instead of the new amplitudes $\vec{b}_{1,2}$ one can use the old amplitudes $\vec{a}_{1,2}$ in these equations.

The ξ dependences given by Eqs. (17), (19)–(21) include a great deal of information on the vectorial coupling. At the first sight, these oscillating dependences look unusual for the nonlocal response which is distinguished by the one-directional energy transfer [2]. Moreover, the possibility for the contrast m to change sign, which formally follows from Eq. (17), seems to be confusing. As a matter of fact, this feature is beyond the field of applicability of the exact relations. It will be shown in the following section that this field is restricted to the region of ξ where $m \geqslant 0$; within this region the propagation coordinate $z = z(\xi)$ ranges from 0 to ∞.

Particular cases

Transverse configuration. Here $\nu_0 = 0$ and the relations (17), (19)–(21) acquire the following simplified form (with the only spatial frequency 2ν present):

$$m = m_0 \cos(2\nu\xi) - F_0 \sin(2\nu\xi),$$
$$F = m_0 \sin(2\nu\xi) + F_0 \cos(2\nu\xi),$$
$$W = W_0 \cos(2\nu\xi) + P_0 \sin(2\nu\xi),$$
$$P = -W_0 \sin(2\nu\xi) + P_0 \cos(2\nu\xi). \tag{23}$$

From here we have

$$m^2(\xi) + F^2(\xi) = m_0^2 + F_0^2, \quad W^2(\xi) + P^2(\xi) = W_0^2 + P_0^2. \tag{24}$$

One sees that m is coupled only with F, W only with P, and instead of the integral $I_p = m^2 + W^2 + F^2 + P^2$ we have two integrals $h_0^2 = m^2 + F^2$ and $g_0^2 = W^2 + P^2$. It is interesting that evolution of the light contrast m is affected by the input value of the polarization characteristic F_0. Depending on F_0, the contrast can be increasing or decreasing function of ξ (and z) near the input face. A similar situation takes place for the intensity difference W; the sign of the derivative $dW/d\xi$ at $\xi = 0$, i.e., the direction of the energy transfer, is controlled by the sign of P_0. For any input values m_0, F_0, W_0, and P_0 the functions given by Eqs. (23) oscillate around zero.

Note that F_0 is expressed by the input intensities of the beams, $I_{1,2}^0$, and the input Stokes vectors $\mathbf{S}_{1,2}^0$, $F_0 = I_1^0(\mathbf{n}\cdot\mathbf{S}_1^0) - I_2^0(\mathbf{n}\cdot\mathbf{S}_2^0)$. If the input polarizations are the same, $\mathbf{S}_1^0 = \mathbf{S}_2^0 = \mathbf{S}_0$, then $F_0 = W_0(\mathbf{n}\cdot\mathbf{S}_0)$ and $P_0 = m_0(\mathbf{n}\cdot\mathbf{S}_0)$. For $m_0 \ll 1$ the value of F_0 can be comparable with one, which means a strong effect of the polarization degrees on the spatial evolution of the contrast.

Let the input beams 1 and 2 be linearly polarized and φ_1 and φ_2 be the corresponding input polarization angles measured from the [001] axis, see Fig. 1(b). Then the input values m_0, W_0, F_0, P_0 can be expressed as follows:

$$m_0 = \sqrt{1 - W_0^2}\cos\varphi_-,$$
$$F_0 = \cos\varphi_+ \sin\varphi_- + W_0 \sin\varphi_+ \cos\varphi_-, \tag{26}$$
$$W_0 = I_1^0 - I_2^0, \quad P_0 = \sqrt{1 - W_0^2}\sin\varphi_+, \tag{27}$$

where $\varphi_\pm = \varphi_1 \pm \varphi_2$. Since the sum of the normalized intensities $I_1^0 + I_2^0 = I_0 = 1$, we have three independent variable input parameters, the normalized intensity difference W_0, and two polarization angles. The integrals h_0^2 and g_0^2 are also functions of these input parameters. The maximum values of h_0^2 and g_0^2, as functions of the angles, occur at $\varphi_{1,2} = \pi/4$ and equal unity. The corresponding minimum values are 0 and W_0^2; they take place at $\varphi_1 = \varphi_2 = \pi/2$.

To illustrate the consequences of Eqs. (26) and (27), we consider again the situation when the input intensities are the same, $W_0 = 0$, whereas the input polarizations are almost perpendicular to each other, $\cos\varphi_- \ll 1$, $m_0 \ll 1$. Here we have $h_0^2 \simeq \cos^2\varphi_+$ and $g_0^2 \simeq \sin^2\varphi_+$. Hence, the maximum attainable values of m and $|W|$ during two-wave coupling are controlled by the sum of the input polarization angles φ_+. They can, by will, be made small or large, see also the following section.

Longitudinal configuration. Here $\nu_0 = \nu$ and we obtain from Eqs. (17) and (19) the following explicit relations for m and W:

$$2m = m_0 - P_0 + (m_0 + P_0)\cos(4\nu\xi) - (W_0 + F_0)\sin(4\nu\xi), \tag{28}$$

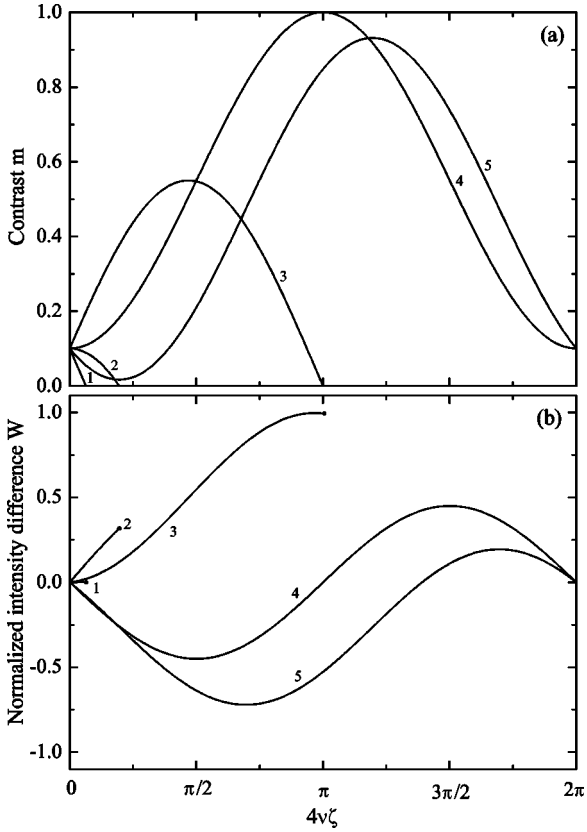

FIG. 3. Dependences $m(\xi)$ and $W(\xi)$ for the L configuration, $m_0=0.1$, and $W_0=0$. The curves 1, 2, 3, 4, and 5 are plotted for the polarization angles $\varphi_+=0$, 90°, 180°, 270°, and 302°, respectively. The dots in (b) mark the limiting values of $W(\xi)$ which correspond to the condition $m(\xi)=0$.

$$2W=W_0-F_0+(m_0+P_0)\sin(4\nu\xi)+(W_0+F_0)\cos(4\nu\xi). \tag{29}$$

Furthermore, one can find from Eqs. (20) and (21) that the polarization characteristics P and F are expressed linearly by m and W:

$$P-P_0=m-m_0, \quad F-F_0=W-W_0. \tag{30}$$

Again we have a strong effect of the polarization degrees of freedom on the coupling characteristics.

To illustrate the polarization effects covered by Eqs. (28)–(30), we consider the case of equal input intensities, $W_0=0$, and linear input polarizations. We can use here Eqs. (26) and (27) to express m_0, F_0, and P_0 by the input polarization angles $\varphi_\pm$. Figure 3 shows the dependences $m(\xi)$ and $W(\xi)$ for several values of φ_+ and a small input value of the contrast, $m_0=\cos\varphi_-=0.1$. For $0<\varphi_+\lesssim\pi/2$ the contrast decreases with ξ and turns to zero at a certain value of the effective coordinate ξ. When φ_+ is increasing, the function $m(\xi)$ experiences a maximum before turning to zero. Then, within the interval $235°\lesssim\varphi_+\lesssim305°$, this function experiences oscillations [likewise the intensity difference $W(\xi)$] and remains positive for any ξ. The value of $[m(\xi)]_{max}$ reaches unity at $\varphi_+\simeq3\pi/2$. For larger values of φ_+ the ξ dependence of the contrast ends up again with a zero value. Thus, we have qualitative different behavior of $m(\xi)$ and $W(\xi)$ depending on the input polarization state.

The same input polarizations meeting the condition $(\mathbf{n}\cdot\mathbf{S}^0_{1,2})=\pm1$. This special choice means that the input vectorial amplitudes $\vec{a}^0_{1,2}\equiv\vec{b}^0_{1,2}$ are the eigenvectors of the interaction matrix, i.e., the vectorial diffraction does not affect the polarization state. In other words, this case corresponds to the scalar beam coupling. The necessary input Stokes vectors correspond to the linear input polarizations. In particular, for the T geometry the corresponding polarization angles are $\varphi=\pm\pi/4$; for the L configuration we have instead $\varphi=0$ and $\pi/2$.

With our choice we have at the input $F_0=\pm W_0$, $P_0=\pm m_0$. One can see from Eqs. (20) and (21) that these relations hold true during propagation, i.e., the variables m and W are sufficient for a complete description. These variables obey the relations

$$m=m_0\cos[2(\nu_0\pm\nu)\xi]-W_0\sin[2(\nu_0\pm\nu)\xi],$$

$$W=m_0\sin[2(\nu_0\pm\nu)\xi]+W_0\cos[2(\nu_0\pm\nu)\xi]. \tag{31}$$

The only difference between the upper and lower signs in Eq. (31) is the value of the effective coupling constant $\nu_0\pm\nu$. In any case we have $m^2+W^2=1$.

One more interesting particular case is the case of identical circular input polarization (left or right) where $(\mathbf{n}\cdot\mathbf{S}^0_{1,2})=0$ and $F_0=P_0=0$. Only isotropic diffraction, which is characterized by the scalar ν_0, takes place here.

V. TRANSITION FROM THE ξ TO z REPRESENTATION

The above exact solutions have been obtained in terms of the effective coordinate ξ which is coupled with the propagation coordinate z by Eq. (12). Since we know the dependence $m(\xi)$, see Eqs. (17), (23), and (28), we can write down in the general case

$$z=\frac{2}{Q|E_0|}\int_0^\xi\frac{d\xi'}{m(\xi')f[m(\xi')]}. \tag{32}$$

This integral can be calculated analytically or numerically for any particular case. A step by step exhaustion of special cases is beyond the scope of this paper. Below we focus our attention on the most important features and consequences of the $\xi\to z$ transition.

Consider first the low-contrast case, $m\lesssim m_c$, where $f(m)\simeq1$, see Sec. II B. For the T geometry, this condition can be fulfilled for any propagation distance if the input parameters are chosen in such a way that $h_0=(m_0^2+F_0^2)^{1/2}\lesssim m_c$. By setting $f=1$ in Eq. (32) and using Eq. (23) for $m(\xi)$, one can obtain the following explicit analytic expression for $z(\xi)$:

$$z=\frac{1}{\Gamma_0}\ln\left[\frac{\tan(\nu\xi_\infty)}{\tan(\nu\xi_\infty-\nu\xi)}\right], \tag{33}$$

where

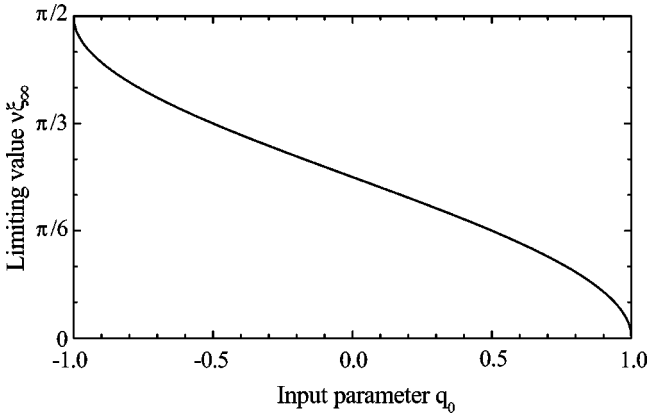

FIG. 4. The limiting value $\nu\xi_\infty$ vs the input parameter q_0 for the T configuration.

$$\Gamma_0 = h_0 Q \nu |E_0| > 0,$$

$$\nu\xi_\infty = \arctan[\sqrt{(1-q_0)/(1+q_0)}],$$

and

$$q_0 = F_0/h_0.$$

The increment Γ_0 characterizes the rate of spatial changes (in z) and ξ_∞ is the limiting value of ξ that corresponds to the first zero point of the function $m(\nu\xi)$ and ranges from 0 to $\pi/2\nu$. The value of $\nu\xi_\infty$ is uniquely expressed by the input parameter q_0, see Fig. 4. The values $\nu\xi_\infty = \pi/2$, 1, and 0 correspond to $F_0 = -h_0$ $(m_0 = 0)$, $F_0 = 0$ $(m_0 = h_0)$, and $F_0 = h_0$ $(m_0 = 0)$, respectively. The same input value of contrast, m_0, corresponds generally to two different values of ξ_∞; this is caused by the fact that the system is not symmetric to the beam interchange in the case of nonlocal PR response.

Figure 5 shows the dependence $\nu\xi(z)$ for several representative values of $\nu\xi_\infty$. One sees that the effective coordinate ξ tends monotonously to its limiting value ξ_∞ when z

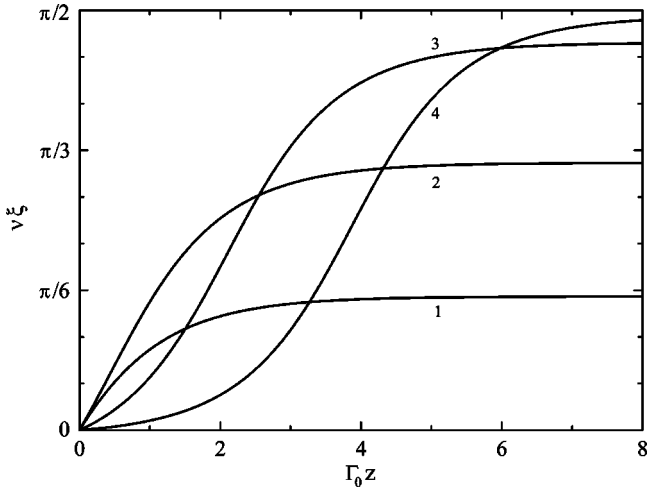

FIG. 5. Dependence $\nu\xi(z)$ for the T geometry. The curves 1, 2, 3, and 4 are plotted for $\nu\xi_\infty = 0.5$, 1.0, 1.45, and 1.55, respectively.

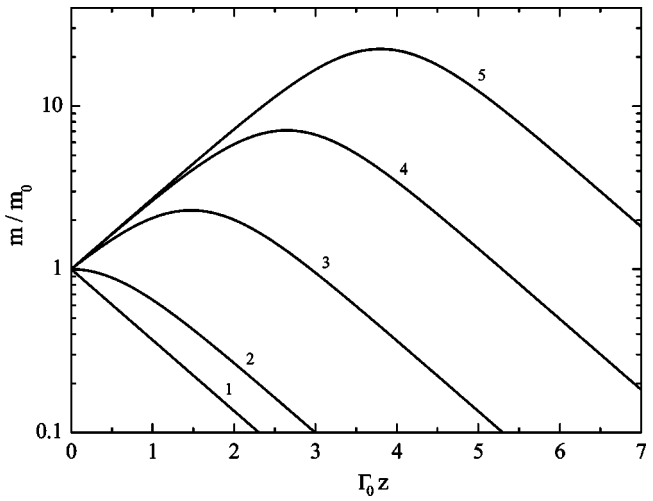

FIG. 6. The ratio m/m_0 vs $\Gamma_0 z$ for the T geometry; the curves 1, 2, 3, 4, and 5 are plotted for $q_0 = 1$, 0, -0.9, -0.99, and -0.999, respectively.

$\to\infty$; with $\nu\xi_\infty$ approaching $\pi/2$ the growth of $\xi(z)$ becomes strongly slowed down in the regions of small and large z (where $m \simeq h_0$).

Next, using Eq. (33), we express by z the trigonometric functions $\sin(2\nu\xi)$ and $\cos(2\nu\xi)$ entering Eqs. (23) and (24) for m, F, W, and P,

$$\sin(2\nu\xi) = \frac{m_0}{h_0}\frac{\sinh(\Gamma_0 z) + q_0\coth(\Gamma_0 z) - q_0}{\coth(\Gamma_0 z) + q_0\sinh(\Gamma_0 z)},$$

$$\cos(2\nu\xi) = \frac{1 + q_0[\sinh(\Gamma_0 z) + q_0\coth(\Gamma_0 z) - q_0]}{\coth(\Gamma_0 z) + q_0\sinh(\Gamma_0 z)}. \tag{34}$$

In the limit $\Gamma_0 z \to \infty$ we have from here $\sin(2\nu\xi_\infty) = m_0/h_0$ and $\cos(2\nu\xi_\infty) = F_0/h_0$.

Now, using Eqs. (23),(24), and (34), one can describe analytically the dependences of m, F, W, and P on the propagation coordinate z. We restrict ourselves to the functions $m(z)$ and $F(z)$,

$$\frac{m}{m_0} = \frac{1}{\coth(\Gamma_0 z) + q_0\sinh(\Gamma_0 z)},$$

$$\frac{F}{F_0} = \frac{1 + q_0^{-1}\tanh(\Gamma_0 z)}{1 + q_0\tanh(\Gamma_0 z)}. \tag{35}$$

The input parameter $q_0 = F_0/\sqrt{F_0^2 + m_0^2}$ entering the right-hand sides of these expressions ranges from -1 to 1. Figure 6 illustrates possible scenarios of the spatial behavior of the light contrast m. For $q_0 > 0$, the contrast monotonously decreases with z tending to zero; if, additionally, $m_0 \ll h_0$ (i.e., $q_0 \simeq 1$), then $m \simeq m_0\exp(-\Gamma_0 z)$. In the case $q_0 < 0$, the function $m(z)$ experiences first a maximum (where $m = h_0$ and $F = 0$) and then tends to zero; if, additionally, $m_0 \ll h_0$, then $m \simeq m_0\exp(\Gamma_0 z)$ at the initial stage of growth.

Qualitatively, the above features are not surprising for the nonlocal response; the regime with an intermediate maxi-

mum corresponds, e.g., to the energy transfer from the initially weakest to the strongest beam. Specific properties (which are not available in the scalar case) are here the possibility to restrict the growth of m from above and to affect the rate and direction of the energy transfer by the polarization degrees of freedom.

To gain an impression about the expected rates of spatial changes, we produce some numerical estimates relevant to ac experiments with BTO crystals. By setting $|s|=4\times10^{-4}\ \mathrm{V}^{-1}$, $|E_0|=20$ kV/cm, and $Q=6$, we have $\nu Q|E_0|\approx 50\ \mathrm{cm}^{-1}$. Despite the fact that $h_0\ll 1$, the product $\Gamma_0 z=h_0 Q\nu|E_0|z$ can easily be made considerably larger than unity.

We continue our analysis of the low-contrast case for the T configuration with specification of the values of F, W, and P that take place for $\Gamma_0 z\gg 1$ ($\xi\to\xi_\infty$). These limiting values are

$$F_\infty=\sqrt{m_0^2+F_0^2},\quad W_\infty=\frac{W_0F_0+m_0P_0}{\sqrt{m_0^2+F_0^2}},$$

$$P_\infty=\frac{P_0F_0-m_0W_0}{\sqrt{m_0^2+F_0^2}}. \tag{36}$$

The limiting value of F coincides, indeed, with that prescribed by Eqs. (35).

It is important that the inequalities $m(z),|F(z)|\leqslant h_0\ll 1$ do not impose severe restriction on the variation range of $W(z)$ and $P(z)$. To make this point clear, we consider the case of equal input intensities ($W_0=0$) and linear input polarizations. The condition $h_0\equiv\sqrt{m_0^2+F_0^2}\ll 1$ can be fulfilled here only for $\cos^2\varphi_\pm\ll 1$; this means either $\varphi_1\simeq\pi/2$, $\varphi_2\simeq 0$ ($\varphi_+\simeq\pi/2$) or $\varphi_1\simeq\pi$, $\varphi_2\simeq\pi/2$ ($\varphi_+\simeq 3\pi/2$). Correspondingly, we have $h_0^2\simeq\cos^2\varphi_+ +\cos^2\varphi_-$ and $q_0=\cos\varphi_+/\sqrt{\cos^2\varphi_+ +\cos^2\varphi_-}$. On the other hand, we have here from Eqs. (26), (28), and (36), $W_\infty=\sqrt{1-q_0^2}\sin\varphi_+\simeq\pm\sqrt{1-q_0^2}$, $P_\infty=q_0\sin\varphi_+\simeq\pm q_0$. Thus, the signs of W_∞ and P_∞ are controlled by the sign of $\sin\varphi_+$ and the absolute value $|W_\infty|$ (or $|P_\infty|$) can approach unity. Figure 7 exhibits the coordinate dependence of the normalized intensity difference. For $q_0>0$ we have a monotonous growth of $W(z)$ up to the value of $\sqrt{1-q_0^2}$. When q_0 changes its sign, the function $W(z)$ shows a maximum ($W_{max}=1$) and then approaches the same limiting value. The nearer q_0 is to -1, the stronger is the shift of this maximum to the right.

Now we extend our study on the whole-contrast range making the main stress on the region $m_c\lesssim m\leqslant 1$ where the function $f(m)$ experiences a strong saturation. The main expected advantage of this region is maintenance of high values of light contrast (because of decreasing rate of energy exchange) during recording. Large values of m, necessary for recording, mean identical input polarizations and comparable intensities. We consider therefore the case where the input polarization vectors are the eigenvectors of the interaction matrix, see Eqs. (31). Then, using Eq. (32) and the notation $\nu_\pm=\nu_0\pm\nu$, we obtain for $m(z)$,

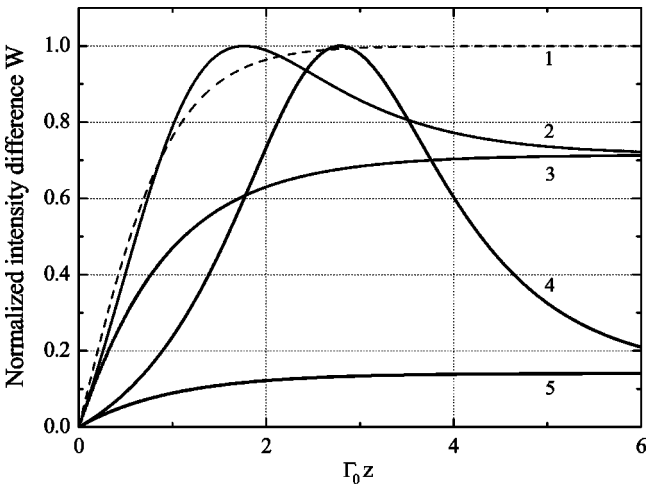

FIG. 7. The normalized intensity difference W vs $\Gamma_0 z$ for the T-geometry and $\sin\varphi_+\simeq 1$; the lines 1, 2, 3, 4, and 5 correspond to $q_0=0$, -0.7, 0.7, -0.99, and 0.99, respectively.

$$\nu_\pm|E_0|z=\int_m^{m_0}\frac{dm}{Qmf(m)\sqrt{1-m^2}}. \tag{37}$$

Figure 8 shows the coordinate dependence of the ratio m/m_0 in a logarithmical scale for several values of m_0 ranging from 0.01 (this belongs the low-contrast region) to unity. For $m_0=0.01$ we have a steep linear decrease which is described by the single-exponential function $m/m_0=\exp(-Q\nu_\pm|E_0|z)$. With increasing m_0, decrease of $m(z)/m_0$ becomes less and less pronounced at the initial stage. As a result, the interval where the recorded index grating remains approximately uniform increases remarkably with m_0. If we define the uniformity range z_u by the equality $m(z_u)=m_0/2$, then we can see that z_u becomes larger by a factor of ≈ 7 when m_0 is increasing from 0.01 to 1. This result may have important consequences for the effects relevant to the grating recording

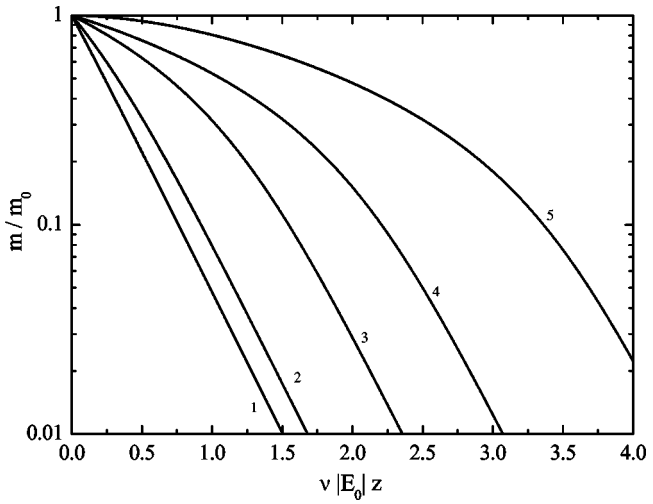

FIG. 8. Dependence $m(z)$ for the scalar case in the whole-contrast range; the curves 1–5 are plotted for $m_0=0.01$, 0.1, 0.4, 0.7, and 1.

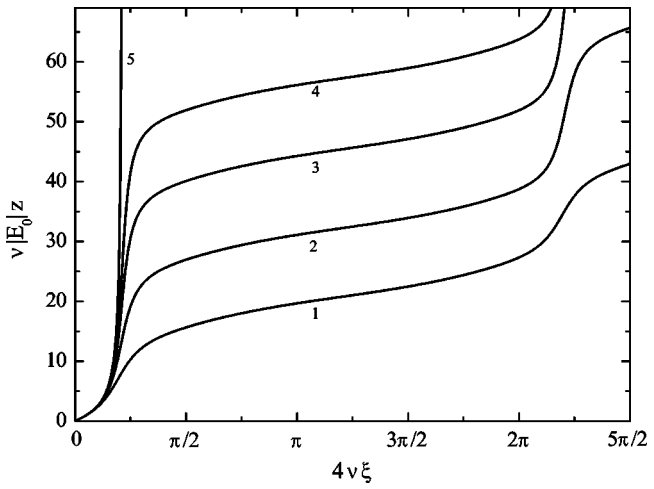

FIG. 9. Dependence $z(\xi)$ for the L configuration. The curves 1–5 correspond to $\varphi_+ = 301.8°$, 304.0°, 304.6°, 304.8°, and 305.1°. Other input parameters are specified in the caption of Fig. 3.

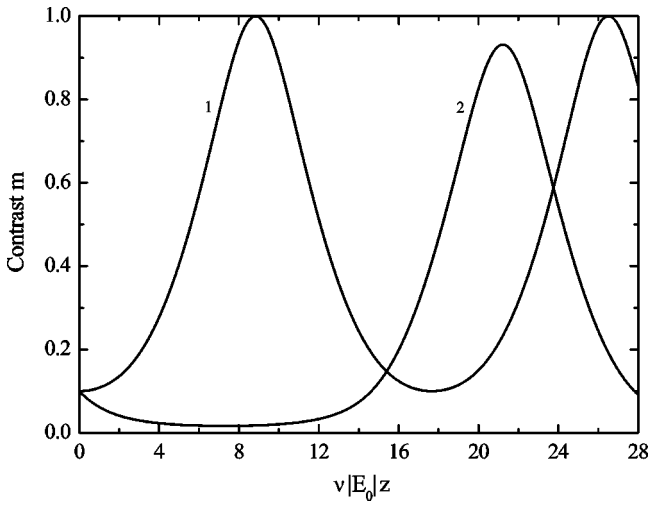

FIG. 10. Dependence $m(z)$ for the L geometry. Curves 1 and 2 are plotted for $\varphi_+ = 270°$ and 302°, respectively.

[32,33]. Moreover, strong coupling effects and recording of quasiuniform gratings can coexist in one sample.

Finally, we consider the $\xi \to z$ transformation for the L configuration. As we know, the contrast m becomes in this case a positive oscillating function of ξ within an interval of the input polarization angles, see Fig. 3(a). This means indeed crossover to periodic dependences $m(z)$ and $W(z)$ and to a qualitatively new dependence $z(\xi)$. Figure 9 shows what happens with the function $z(\xi)$ when the input polarization angle φ_+ increases from 301.8° to 305.1° (transition from periodic to nonperiodic states occurs at $\varphi_+ \simeq 305°$). For $\varphi_+ < 305°$ the function $z(\xi)$ is finite and single valued. It shows a linear growth superimposed by strong periodic oscillations. The average slope tends to infinity when φ_+ is approaching 305°. At $\varphi_+ = 305.1°$ the propagation coordinate z tends to infinity for $\xi \to \xi_\infty$; the limiting value ξ_∞ is, as earlier, the first zero point of the function $m(\xi)$.

The lines 1 and 2 in Fig. 10 correspond to the lines 4 and 5 in Fig. 3(a) and exhibit the periodic behavior of the light contrast. Nontrivial and strong periodic oscillations of $m(z)$ originate from harmonic oscillations of $m(\xi)$. The oscillation period for the curve 2 is considerably larger than that for the curve 1. This is fully due to proximity of the curve 5 in Fig. 3(a) to zero. With φ_+ increasing, this curve touches the horizontal; the period of oscillation becomes here infinitely long and the periodic oscillations of $m(z)$ transform into a monotonous decrease.

VI. SUMMARY

The main findings of this paper can be summarized as follows:

(a) Vectorial two-wave coupling caused by the ac enhanced nonlinear response possesses different quantitative properties in the regions of low $(0 \leqslant m \lesssim m_c \ll 1)$ and high $(m_c \lesssim m \leqslant 1)$ light contrast m. The narrow low-contrast range is optimum for the spatial amplification of weak waves, while the high-contrast region is preferable for recording of refractive index gratings.

(b) The light interference fringes experience neither bending nor tilting during vectorial two-wave coupling under ac field; this result is valid in the whole-contrast region irrespective of the input polarizations of the interacting waves.

(c) Owing to this property of the light fringes and under certain assumptions on the coupling characteristics (applicable, e.g., to BTO crystals and crystals of the $\overline{4}3m$ point group), the nonlinear problem of vectorial coupling is reduced to a linear problem of vectorial Bragg diffraction; the latter admits an exact solution.

(d) Analysis of the auxiliary linear problem has shown the presence of an additional (to the energy conservation law) integral of motion which involves the polarization degrees of freedom; this analysis is not restricted to any particular contrast range.

(e) Consideration of particular cases relevant to experiment has allowed to reveal the possibilities for further simplifications of vectorial equations and predict a number of new regimes with a strong influence of the input polarizations on the output energy and polarization characteristics.

We expect that the above findings will stimulate further ac experiments on vectorial beam coupling in the sillenites. Furthermore, the results obtained can be of importance for development optimization of the novel technique for detection of weak signals [32,33] based on the ac-enhanced vectorial beam coupling. From the fundamental point of view, the above theory fills the gap in the studies of vectorial wave coupling in cubic crystals.

ACKNOWLEDGMENT

Financial support from Deutsche Forschungsgemeinschaft is gratefully acknowledged.

[1] M.P. Petrov, S.I. Stepanov, and A.V. Khomenko, *Photorefractive Crystals in Coherent Systems* (Springer-Verlag, Berlin, 1991).
[2] L. Solymar, D.J. Webb, and A. Grunnet-Jepsen, *The Physics and Applications of Photorefractive Materials* (Clarendon Press, Oxford, 1996).
[3] P. Refregier, L. Solymar, H. Rajbenbach, and J.-P. Huignard, J. Appl. Phys. **58**, 45 (1985).
[4] S.I. Stepanov and M.P. Petrov, Opt. Commun. **53**, 292 (1985).
[5] C.S.K. Walsh, A.K. Powell, and T.J. Hall, J. Opt. Soc. Am. B **7**, 288 (1990).
[6] A.A. Kamshilin, T. Jaaskelainen, C.J. Lima, M.R.B. Andreeta, and V.V. Prokofiev, Opt. Lett. **18**, 690 (1993).
[7] A.A. Kamshilin, R. Ravattinen, H. Tuovinen, T. Jaaskelainen, and V. Prokofiev, Opt. Commun. **103**, 221 (1993).
[8] E. Raita, A.A. Kamshilin, V.V. Prokofiev, and T. Jaaskelainen, Appl. Phys. Lett. **70**, 1641 (1997).
[9] A.A. Kamshilin, E. Raita, and A.V. Khomenko, J. Opt. Soc. Am. B **13**, 2536 (1996).
[10] A.A. Kamshilin, E. Raita, and T. Jaaskelainen, Opt. Rev. **3**, 443 (1996).
[11] E. Shamonina, K.H. Ringhofer, B.I. Sturman, G. Cedilnik, A. Kießling, R. Kowarschik, A.A. Kamshilin, V.V. Prokofiev, and T. Jaaskelainen, Opt. Lett. **23**, 1435 (1998).
[12] A.A. Kamshilin, Y. Iida, S. Ashihara, T. Shimura, and K. Kuroda, Appl. Phys. Lett. **74**, 2575 (1999).
[13] A. Marrakchi, R.V. Johnson, and A.R. Tanguay, J. Opt. Soc. Am. B **3**, 321 (1986).
[14] S. Mallick, D. Rouède, and A.G. Apostolidis, J. Opt. Soc. Am. B **4**, 1247 (1987).
[15] B.I. Sturman, D.J. Webb, R. Kowarschik, E. Shamonina, and K.H. Ringhofer, J. Opt. Soc. Am. B **11**, 1813 (1994).
[16] J.R. Goff, J. Opt. Soc. Am. B **12**, 99 (1995).
[17] N.V. Kukhtarev, G.E. Dovgalenko, and V.N. Starkov, Appl. Phys. A: Solids Surf. **33**, 227 (1984).
[18] S. Mallick and D. Rouède, Appl. Phys. B: Lasers Opt. **43**, 239 (1987).
[19] E. Shamonina, V.P. Kamenov, K.H. Ringhofer, G. Cedilnik, A. Kießling, and R. Kowarschik, J. Opt. Soc. Am. B **15**, 2552 (1998).
[20] J. Kumar, G. Albanese, and W.H. Steier, J. Opt. Soc. Am. B **4**, 1079 (1987).
[21] I. Auberecht, H.C. Ellin, A. Grunnet-Jepsen, and L. Solymar, J. Opt. Soc. Am. B **12**, 1918 (1995).
[22] A.A. Izvanov, A.E. Mandel, N.D. Khatkov, and A.E. Shandarov, Optoelectronics **2**, 80 (1986).
[23] V.V. Shepelevich, S.M. Shandarov, and A.E. Mandel, Ferroelectrics **110**, 235 (1990).
[24] G. Pauliat, P. Mathey, and G. Roosen, J. Opt. Soc. Am. B **8**, 1942 (1991).
[25] M. Zgonik, K. Nakagava, and P. Günter, J. Opt. Soc. Am. B **12**, 1416 (1995).
[26] H. Touvinen, A.A. Kamshilin, R. Ravattinen, V. Prokofiev, and T. Jaaskelainen, Opt. Eng., **34**, 2641 (1995).
[27] H.C. Pedersen and P.M. Johansen, J. Opt. Soc. Am. B **12**, 592 (1996).
[28] H. Tuovinen, A.A. Kamshilin, and J. Jaaskelainen, J. Opt. Soc. Am. B **14**, 3383 (1997).
[29] B.I. Sturman, E.V. Podivilov, K.H. Ringhofer, E. Shamonina, V.P. Kamenov, E. Nippolainen, V.V. Prokofiev, and A.A. Kamshilin, Phys. Rev. E **60**, 3332 (1999).
[30] B.I. Sturman, A.I. Chernykh, V.P. Kamenov, E. Shamonina, and K.H. Ringhofer, J. Opt. Soc. Am. B **17**, 985 (2000).
[31] L.D. Landau and E.M. Lifshiz, *Quantum Mechanics* (Pergamon Press, Oxford, 1969).
[32] K. Paivasaari, A. Kamshilin, V.V. Prokofiev, B. Sturman, G.F. Calvo, M. Carrascosa, and F. Agullo-Lopez, J. Appl. Phys. **90**, 3135 (2001).
[33] G.F. Calvo, B. Sturman, M. Carrascosa, F. Agullo-Lopez, K. Paivasaari, and A. Kamshilin, J. Opt. Soc. Am. B **19**, 1564 (2002).
[34] B.I. Sturman, M. Mann, J. Otten, and K.H. Ringhofer, J. Opt. Soc. Am. B **10**, 1919 (1993).
[35] L.D. Landau and E.M. Lifshiz, *Field Theory* (Pergamon Press, Oxford, 1969).
[36] M. Born and E. Wolf, *Principles of Optics* (Pergamon Press, London, 1959).
[37] G.A. Brost, J. Opt. Soc. Am. B **9**, 1454 (1992).
[38] J.E. Millerd, E.M. Garmine, M.B. Klein, B.A. Wechsler, F.P. Strohkendl, and G.A. Brost, J. Opt. Soc. Am. B **9**, 1449 (1992).
[39] O. Fillipov, K.H. Ringhofer, and B.I. Sturman, Eur. Phys. J. D **23**, 285 (2003).